

UNCLASSIFIED

SLL 80 619
copy 1

File: Bell@ . m 2761

30

LASER
CL, P

**MODELING C.W. DF AND HF LASER PERFORMANCE
AT LOW CAVITY PRESSURES AND DILUENT CONDITIONS**

W.L. Rushmore and S.W. Zelazny

NIAGARA FRONTIER OPERATIONS

Bell Aerospace **TEXTRON**

Division of Textron Inc.

Buffalo, New York 14240

AIAA Paper No. IV-5

AIAA Conference On
Fluid Dynamics of High Power Lasers
Cambridge, Massachusetts

OCTOBER 31 - NOVEMBER 2, 1978

PLEASE RETURN TO:

**BMD TECHNICAL INFORMATION CENTER
BALLISTIC MISSILE DEFENSE ORGANIZATION
7100 DEFENSE PENTAGON
WASHINGTON D.C. 20301-7100**

DTIC QUALITY INSPECTED 43

19980309 300

u4022

UNCLASSIFIED

DISTRIBUTION STATEMENT A
Approved for public release;
Distribution Unlimited

Accession Number: 4022

Publication Date: Nov 02, 1978

Title: Modeling CW DF and HF Laser Performance at Low Cavity Pressures and Diluent Conditions

Personal Author: Rushmore, W.L.; Zelazny, S.W.

Corporate Author Or Publisher: Bell Aerospace TEXTRON, Buffalo, NY 14240 Report Number: AIAA Paper No. IV-5 Report Number Assigned by Contract Monitor: SLL 80 619

Comments on Document: Archive, RRI, DEW. Presented at the AIAA Conference on Fluid Dynamics of High Power Lasers, Cambridge, MA, October 31-November 2, 1978

Descriptors, Keywords: Model Continuous Wave Hydrogen Deuterium Fluoride Laser Performance Low Cavity Pressure Diluent Condition Geometry Flow Area Expansion Chemiluminescence Vacuum Duct Pressure Chemical

Pages: 00039

Cataloged Date: Dec 07, 1992

Document Type: HC

Number of Copies In Library: 000001

Record ID: 25501

Source of Document: DEW

MODELING C.W. DF AND HF LASER PERFORMANCE
AT LOW CAVITY PRESSURES AND DILUENT CONDITIONS*

W.L. Rushmore[†] and S.W. Zelazny[‡]

Bell Aerospace **TEXTRON** Buffalo, New York

Division of Textron Inc.

Abstract

A laser performance model originally developed for high cavity pressure and diluent c.w. lasers is extended to apply to a significantly lower pressure and diluent operating regime. The different class of laser nozzle geometries used in low diluent applications are described and a method for theoretically modeling the internal flow area expansion which occurs in these designs is presented. Experimental data (closed cavity power, chemiluminescence, zero power gain) for helium diluent hydrogen fluoride and nitrogen diluent deuterium fluoride chemical lasers is used to assess the accuracy of the model. Agreement between theory and data is good for both the axisymmetric and two dimensional nozzle geometries examined. Test conditions where theory and data do not agree are shown to be in part related to the influence of shroud geometry and vacuum duct pressure on the flowfield.

Nomenclature

- A = Laser nozzle face area
 \dot{m} = Mass flow
 $(\dot{N}_{F_2})_A$ = Total molar flowrate of available fluorine, $\dot{N}_F/2 + \dot{N}_{F_2}$
 N_i = Molar flowrate of specie i
 p'_7 = Recoverable pressure at diffuser exit

Presented at the AIAA Conference on Fluid Dynamics of High Power Lasers, Cambridge, Mass.,
October 31,-November 2, 1978.

Index Categories: Lasers: Reactive Flows

*Work supported in part under MIRADCOM Contract DAAK40-76-C-1059 and Bell Aerospace
Textron Independent Research and Development Program.

[†]Research Scientist, High Energy Lasers, Member AIAA

[‡]Staff Scientist, High Energy Lasers, Member AIAA

p_c	= Combustor pressure
p_I	= Nozzle exit pressure
P_{TOT}^{DF*}	= Total outcoupled power for DF* lasing
$P_{v-(v-1)}$	= Outcoupled power for lasing from v to $v-1$ vibrational level
$P_v(J)$	= Small signal gain for lasing from $v+1$ to v vibrational level, on rotational line J
Re	= Reynolds number based on stagnation conditions and nozzle radius or half height
R_L	= Cavity molar mixture ratio
T_{oc}	= Combustor total temperature
T_{oI}	= Total temperature at injector exit
V	= Axial velocity
x	= Axial coordinate
x_c	= Axial location of optimum stable resonator axis
β_c	= Combustor molar diluent ratio
β_{N_2}	= Combustor molar diluent ratio of N_2
β_s	= Cavity molar diluent ratio
δ	= Power flux per unit area
Ω	= Total (combustor plus cavity) diluent ratio
σ	= Specific power based on combustor and lasing nozzle mass flow
$\bar{\sigma}^*$	= Molar specific power/reference molar specific power, see ref. 2 for reference value.

I. Introduction

The Problem

The basic components of a chemical laser are shown schematically in Figure 1. In an earlier study¹, a theoretical model was described which predicted the closed cavity power in continuous wave (c.w.) HF and DF lasers. The operating regime examined in that study¹ was generally characterized by mass throughputs, \dot{m}/A , greater than 1.0 g/s-cm^2 and high diluent levels ($\Omega > 30$). Also, the laser nozzle designs considered in this earlier study¹ contained very little internal area relief for flow expansion induced by heat release in the laser cavity. Comparison of the schematics of the low base relief BCL-7 and high base relief BCL-13 nozzles shown in Figure 2 illustrates the difference between the two types of nozzle concepts.

The high base relief nozzle has practical application in laser systems which must achieve high power extraction efficiency at low diluent levels. In addition, these laser systems only require relatively low pressure recovery capability (30 torr or less). The specific problem addressed in this study was to evaluate the capability of the laser performance analysis technique¹ developed for high pressure, high diluent lasers to characterize this significantly different operating regime and to improve the model where necessary.

Approach

A number of investigations²⁻⁶ have been made which provide closed cavity power, chemiluminescence measurements, and zero power gain data for the operating regime of interest, i.e., low diluent and cavity pressures. Two approaches have been used to evaluate the ability of a laser model to characterize details of the laser flowfield. The first approach uses one particular nozzle geometry and operating condition⁷, whereas the second approach uses a number of nozzle geometries and operating conditions¹. We have selected the second approach in this study. The governing equations, method of solution, and technique used to establish the conditions at the cavity entrance plane are identical to those described by Zelazny et al¹.

The data base²⁻⁶ used in this study is described in Section II. Details of the analyses used to consider influences of the base area, stable resonator geometry and cavity pressure distributions are given in Section III. Results are given in Section IV followed by the main conclusions of this investigation, Section V.

II. Data Base

A summary of the data reviewed in this study is given in Table 1. The axisymmetric nozzles BCL-13 and BCL-14 are shown schematically in Figure 3, whereas the two-dimensional nozzle LRC-1 and quasi-axisymmetric nozzle LRCL-2 are shown in Figure 4. The LRCL-2B nozzle differs from the LRCL-2 nozzle in that the sonic lasant injection orifices of LRCL-2 were modified to supersonic conical nozzles in the LRCL-2B configuration⁴. This design (LRCL-2 and 2B) is herein referred to as a quasi-axisymmetric nozzle since unlike the BCL-13 and 14 designs it does have azimuthal variations in the lasant flowfield around the circumference of the circular primary nozzle due to the discrete orifice injection configuration.

The data to be examined can be conveniently subdivided into helium diluent hydrogen fluoride data and nitrogen diluent deuterium fluoride data designated as He-HF* and N₂-DF*. Three types of data are available (1) closed cavity power (CCP) obtained with a stable resonator which is used to determine the optimum optical axis (x_c) and provide an approximate measure of the lasing zone length ($2x_c$); (2) chemiluminescence data giving the number density and rotational temperature distribution in the lasing zone and (3) zero power gain distributions in the flow direction on the nozzle centerline.

The laser performance may be expressed in terms of the following flow parameters: (1) mass throughput, \dot{m}/A , (2) combustor diluent level, β_c , (3) adiabatic flame temperature in the combustor, T_{OI} , (4) cavity mixture ratio, R_L , and (5) diluent level in the lasant stream, β_s . Examination of the experimental data base shows how performance varies with these parameters for a given nozzle geometry. Results of the theoretical model predictions are compared with the experimentally observed trends in Section IV.

III. Analysis

Either two-dimensional or axisymmetric flowfields are considered and the boundary layer approximations are assumed to apply. A quasi-two-dimensional form of these equations were obtained¹ and solved using implicit integration techniques by the BLAZE-II Computer Code. Starting conditions at the nozzle exit plane were computed using the CNCDE computer code developed by Driscoll⁸ where viscous losses induced by the nozzle boundary layers are considered for both the primary and secondary nozzles. Combustor heat loss and totally regeneratively cooled nozzle designs, e.g., BCL-13, are considered by transferring the primary nozzle heat loss to the secondary nozzle to raise the lasant stagnation temperature. The following subsections describe features of the analysis which have been included to account for nozzle designs used in the low pressure and diluent operating range of interest in this investigation.

Considering Base Area Effects

Figure 5 shows a schematic of the side view of an axisymmetric or two-dimensional (slit) nozzle which contains a significant base region. A number of studies, e.g. ref 9, have examined the details of the flowfield which include the influence of transverse pressure gradients, flow separation of the primary and/or secondary nozzle and the recirculation zone in the base region. Unfortunately, the elliptic equation system required to include these influences requires considerable computer

solution time and the resulting models cannot be readily used to conduct extensive parametric studies to establish the trends needed to guide experimental test plan definition. The model used herein uses a parabolic equation system and assumes the pressure across the mixing, reacting, and lasing region is constant. Hence, transverse pressure gradients and recirculation effects have been neglected. As a consequence of neglecting these effects, it becomes necessary to develop a technique which allows a reasonable definition of effective (or idealized) nozzle exit plane conditions. Specifically, the flow and geometric parameters which must be defined are an average static pressure, effective primary and secondary nozzle exit dimensions (the mixing scales) and temperature and velocity boundary layer profiles which reflect the flow expansions and/or compressions consistent with the average pressure. These parameters are computed as follows. For a sonically injected lasant stream, the flow is assumed to expand outwards into the base region until its pressure is matched with the primary nozzle exit pressure. This implies that the primary nozzle exit pressure is the critical pressure for the cavity mixing calculation. The initial laminar mixing length scale for the secondary nozzle is then taken to be the sum of the expanded secondary nozzle dimension plus the remaining base dimension. As will be shown in Section IV, these assumptions allow the theoretical predictions for the main flow features and gain distributions to be accurately correlated with the experimental observations. It is the treatment of the internal base region which accounts for the principal difference in modeling high pressure (as in ref. 1) and low pressure flows. As the internal base approaches zero, the two models become equivalent.

The pressure distribution in the laser cavity is a function of the imposed boundary condition. Unless specifically identified, the results presented herein assume a constant pressure cavity until the internal base is filled. From this point on, a constant area flow (equal to the laser nozzle face area A) is assumed and hence a subsequent pressure rise is computed. It should be pointed out that a freejet flow, i.e., an unshrouded laser flow which surrounds the laser pressure field with the vacuum duct pressure, is not equivalent to a constant pressure flow in that the bulk average pressure in a freejet flow can decrease if the exit flow is underexpanded.

Closed Cavity Power

The closed cavity power is computed using a Fabry-Perot optical cavity and the gain equals loss assumption is made. The mirror reflectivities are specified as input parameters. A laminar mixing model is used which takes into account the local pressure and temperature to compute a

laminar diffusion coefficient. Rotational equilibrium is assumed for all vibrational states (see Sentman¹⁰ for a discussion on the consequences of this assumption). The DF kinetics are the same as those used in ref. 1 and are given in Table 2. The HF kinetics are those given in ref. 11, and are listed in Table 3. Calculations were made assuming either full F-atom recombination or negligible F-atom recombination on the nozzle wall at the cavity entrance plane. The effect of the F-atom recombination assumption will be shown in the results section. Upstream/downstream coupling effects induced by the stable resonator configuration which reduce laser closed cavity power due to the propagation of radiation through regions of negative gain (absorption zones) are obviously not considered in the Fabry-Perot model. An approximate method of accounting for this influence in this model will be described in the following section.

IV. Results

N₂-DF* Data and Theory Comparisons

Closed cavity power and chemiluminescence data was described by Zelazny et al² for the two axisymmetric nozzles BCL-13 and 14 shown in Figure 3. Both nozzles have identical primary and secondary dimensions and differ only in the nozzle packing density. The BCL-13 nozzle has 45 nozzles/in², whereas BCL-14 has 33 nozzles/in². Consequently, the BCL-14 nozzle provides 12% more base region for flow expansion than the BCL-13 array but requires combustor pressures 36% greater than BCL-14 to achieve the same mass flowrate.

Figure 6 shows the rotational temperature distribution with distance downstream obtained from the chemiluminescence data for BCL-13. Also shown are the predictions using the C/B (i.e., CNCDE-BLAZE-II) computer code with various methods considered for treating the internal base. The baseline curve is obtained using the assumptions outlined in Section III, i.e., the secondary flow expands to a matched pressure and its laminar mixing scale length is the entire base dimension. Two other methods for modeling the base region were examined, and results are also shown in Figure 6. In one method the laminar mixing length scale of the secondary nozzle was taken as that dimension required to obtain a matched pressure with the primary nozzle flow. The second method used the entire base region for complete expansion of the nozzle flow at the nozzle exit plane before the reaction commences. A matched pressure plus primary and secondary length scales are then determined based on the total nozzle bank area available to the flow. As can be seen, the baseline

curve follows the data much more closely, particularly in the first centimeter where the majority (> 75%) of the power is extracted.

Detailed closed cavity power data for BCL-14 was used to compare theory with data. Parametric studies were conducted using the BCL-14 nozzle varying p'_7 (i.e., the recoverable pressure assuming 80% normal shock recovery in a constant area supersonic diffuser), combustor inlet temperature T_{OI} , combustor molar diluent level β_{N_2} , cavity molar mixture ratio R_L , and cavity molar diluent ratio β_s . The recoverable pressure is directly correlatable with the mass throughput at a fixed T_{OI} , β_{N_2} , R_L , and β_s as shown in Figure 7 for the BCL-13 and 14 nozzle designs.

Figure 8 shows the predicted power-on gain profiles for BCL-14. The gain curves are for transitions from the $v=1$ to $v=0$ lines for various J values. As a consequence of the rotational equilibrium assumption, the power is computed such that extraction can only occur from one J value at a time for each vibration line¹⁰. As a result, the lower J values enter an absorption condition while power is being extracted from the higher J levels.

This neglecting of multiline lasing and the potential for the radiation intensity propagated from a positive gain region through an absorption zone downstream represents a significant shortcoming of the current model. The result of this limitation is that laser power predictions made assuming an optical cavity composed of plane parallel mirrors will allow power extraction on lines which will not achieve saturation in stable resonators containing concave mirror geometries. A very simple yet effective method for approximating this effect without resorting to costly (increased computer time) modifications to the resonator model is to reduce the power extraction efficiency of the Fabry-Perot cavity prediction. Here, we uniformly downgrade the power extraction obtained on the $v=3-2$, $2-1$, and $1-0$ transitions by 15% based on comparisons between theory and data.

Figure 9 shows the C/B comparisons with BCL-14 data for a p'_7 (i.e., \dot{m}/A) scan. Two prediction curves are presented. One was made assuming complete F-atom recombination on the nozzle wall, whereas the second was made assuming no F-atom recombination. As can be seen, the complete recombination results agree much better with the $\bar{\sigma}^*$ and x_c data. For this reason, the remainder of the C/B N_2 -DF* predictions are made with complete recombination. Figure 10 shows the results for a T_{OI} scan. The predictions correctly show the increase of $\bar{\sigma}^*$ with T_{OI} to within 10% of the data. Figure 11 shows the β_{N_2} scan results. The data shows that $\bar{\sigma}^*$ remains

essentially constant as β_{N_2} is raised from 1.0 to 8.0, while the C/B predictions show a 20% drop in $\bar{\sigma}^*$. However, the predictions do correctly show the increase in x_c with β_{N_2} . Figure 12 shows the results of the R_L scan. BCL-14 was designed to operate in either the regeneratively cooled mode (i.e., the secondary nozzle flow is used to cool the complete nozzle bank) or the dump cooled mode (where some of the secondary flow is dumped externally from the cavity). In this way low R_L values could be run in the dump cooled mode. For the data of Figure 12, the $R_L = 5.0$ and 10.0 conditions were run in the dump cooled mode. The CNCDE code may also be run in the dump cooled mode (i.e., the heat transfer from the primary flow to the secondary flow is controlled), so the C/B predictions for $R_L = 5.0$ and 10.0 were also made in the dump cooled mode. As can be seen, the increase in $\bar{\sigma}^*$ as R_L decreases is correctly predicted to within 18%. Finally, Figure 13 shows the results for the β_s scan. The data and theory both show no benefit in increasing β_s and an insensitivity of lasing zone length to β_s .

Comparisons between theory and data for the BCL-13 nozzle showed results similar to those obtained with the BCL-14 nozzle comparisons. The theory showed that the BCL-13 design would yield approximately 15% higher efficiency than the BCL-14 nozzle at comparable throughput conditions. Table 4 shows a comparison between theory and data for the BCL-13 nozzle at a high performance condition.

He-HF* Data and Theory Comparisons

Closed cavity power data for the LRCL-1, 2, and 2B nozzles in a freejet configuration were examined. The LRCL-1 two-dimensional and LRCL-2 axisymmetric nozzle geometries are shown in Figure 4. The LRCL-2 nozzle is different from the BCL-13 and BCL-14 axisymmetric nozzles in that the LRCL-2 secondary nozzles consist of six sonic orifices equally spaced around the primary nozzle, whereas the BCL-13 and 14 axisymmetric secondary nozzles consist of a concentric circular orifice (see Figure 3). The LRCL-2 nozzle was modeled as a "true" axisymmetric in that an equivalent area concentric secondary nozzle was assumed. The LRCL-2B nozzle has an identical primary nozzle to LRCL-2 with six supersonic secondary nozzles with an area ratio of 16.0. Again, this was modeled as an equivalent throat and exit area concentric ring.

Comparisons of C/B predictions with the zero power gain data for LRCL-2 are shown in Figures 14 and 15 for the $P_1(6)$ and $P_2(5)$ lines. The effect of F-atom wall recombination on the nozzle wall at the exit plane is also examined. As was the case for the BCL-14 power data, the

complete F-atom recombination predictions follow the data much more closely. The C/B runs were made assuming a constant area cavity boundary condition. The internal base was sufficient so that all runs predicted a constant pressure flow to 5 cm. The data was taken in a freejet configuration, and as stated previously, this may not be equivalent to a constant pressure cavity flow if the vacuum duct pressure is lower than the nozzle exit pressure. This may explain why the P₁(6) data has a longer positive gain region than the predictions. The P₂(5) data, which goes into absorption sooner, is closely tracked by the C/B predictions.

Figure 16 shows the number density data for HF(1) and HF(2) compared with the C/B predictions. Again, the complete recombination results track the data much more closely than the no recombination results, particularly for HF(2). Therefore, the remainder of the C/B runs for He-HF* are also made with complete F-atom wall recombination. Figure 17 shows the zero power gain results for LRCL-1 for the P₁(7) and P₂(7) lines. While the C/B predictions are not in as good agreement as for LRCL-2, the peak gains are still predicted to within 1.5%/cm and the location of the peak gain to within 0.5 cm.

The argument made for N₂-DF lasers that upstream/downstream coupling effects due to absorption will degrade the actual power is also relevant to the HF data examined. Hence, the C/B power predictions were degraded by 25% to give good agreement between theory and data. Specifically, the following relation was used.

$$p_{\text{Tot}}^{\text{HF}^*} = 0.75 (p_{1-0}^{\text{HF}^*} + p_{2-1}^{\text{HF}^*})$$

It is seen from the above relationship that for DF lasing the power available is obtained from three levels, whereas for HF lasing it is available from only two levels.

The freejet data for LRCL-1, 2 and 2B was examined and the results are presented in Figure 18. The LRCL-2B model requires some further discussion. As stated in Section III, the sonic secondary flow was allowed to expand into the base region until a matched pressure with the primary nozzle flow is obtained. For the supersonic secondary LRCL-2B nozzle, the secondary nozzle exit pressure was typically only 10 to 20% that of the primary nozzle. Since the BLAZE-II code cannot consider transverse pressure gradients explicitly, the initial pressure for the laminar mixing calculations was taken as the primary nozzle pressure since the dominant mixing mechanism is the diffusion of H₂ into the primary flow.

At the lower flowrates ($\dot{m}/A = 0.05$ and 0.10), the C/B predictions are within 10% of the data and correctly predict that LRCL-2 gives the best performance (i.e., σ) with LRCL-1 and LRCL-2B giving almost equivalent specific power σ . At the higher flowrates, the C/B predictions start falling off and give significantly lower σ 's than measured. A possible explanation for this result is that in a freejet configuration the influence of the lower vacuum duct pressure will have more of an influence at higher \dot{m}/A (i.e., higher exit pressures). The initial C/B runs were made with a constant area cavity boundary condition. The LRCL-2 and LRCL-2B predictions show adequate internal base to allow constant pressure cavity flow at all flowrates. However, the LRCL-1 predictions show that the flow will choke at the higher \dot{m}/A 's of 0.29 and 0.35 g/cm^2 . Therefore, these conditions were rerun with a linear area expansion of 15% over 10 cm, which was adequate to predict a constant pressure cavity flow, see Figure 18.

The effect of the cavity boundary conditions are further examined in Figure 19. Two additional sets of calculations for LRCL-2 were made. Both assumed that the cavity pressure decreases from the nozzle exit pressure to a value of 1 torr at 5 cm downstream. One set of runs assumed a linear decrease, while the second set assumed a parabolic decrease (i.e., the pressure drops off faster in the initial region than the case using a linear profile.) As can be seen, the predictions with the faster (parabolic) decrease in pressure show the same trend as the data in that the specific power no longer drops off sharply with increasing \dot{m}/A . Thus the cavity boundary condition has a marked effect when considering the scalability of the data to larger nozzle dimensions. Table 5 shows a comparison of the measured and predicted x_c 's for the data of Figures 18 and 19. As can be seen, the predicted x_c 's are typically 40-70% shorter than the measured values when a constant area boundary condition is employed; however, when the parabolic decrease in pressure boundary condition was used, the predicted x_c 's for LRCL-2 increase and are much closer to the measured values.

A number of uncertainties in the accuracy of the reaction rate models exist and hence it was of interest to determine the sensitivity of computed laser performance to changes in various rate constants for a low pressure He-HF laser. The test conditions chosen were for LRCL-2 at a low \dot{m}/A , since both the predicted gain and performance were both in good agreement with experimental data. The results are given in Table 6. Different sets of rates were examined individually with respect to the baseline rates. Multiplying or dividing the pumping rates by a factor of two had the expected

result of increasing and decreasing the predicted specific power. In all cases doubling the deactivation rates also decreased specific power. However, the net effect was always less than 10%.

V. Conclusions

(1) A direct extension of the model developed in low base nozzles designed for high cavity pressure operation¹ was found to inadequately characterize the rate of mixing between the lasant and primary streams of high base nozzles. Numerical experimentation showed that the mixing scale required to accurately describe the entrainment of the lasant into the mixing region was the width of the base region rather than the lasant nozzle exit dimension.

(2) Comparisons between theory and zero power gain and chemiluminescence data showed that the model accurately predicted the experimentally observed trends and was in good agreement with the absolute magnitude of the measured zero power gains.

(3) Theoretical comparisons with closed cavity power data showed the theory to overestimate power by approximately 15% for most DF conditions and 25% for HF tests. The assumption of plane parallel mirrors (Fabry-Perot model) will in part account for the overly optimistic predictions as will the assumption of rotational equilibrium.^{10,12}

(4) The C/B model accurately predicted the observed variations in laser performance with the dependent flow parameters (mass throughput, temperature, diluent level, and cavity mixture ratio).

(5) The current version of the C/B computer code has been shown to give accurate predictions for low pressure, high base nozzles for a wide range of flow conditions. The effect of F-atom wall recombination has been shown to be an important mechanism in that both the BCL-14 power/ x_c and the LRCL-2 gain data are both accurately predicted assuming complete F-atom recombination. The results of the kinetic model sensitivity study show the predictions to be insensitive to factors of two changes in various rates.

(6) The simplicity of the model has required that a number of assumptions be made to keep the computer solution time reasonable. Physical processes which have not been considered explicitly but which have been or are currently being incorporated in various computer codes at Bell Aerospace Textron are: (i) rotational nonequilibrium effects, (ii) upstream-downstream coupling influence of stable resonators, (iii) transverse pressure gradient effects, (iv) fully viscous primary and secondary nozzle flow influences on cavity entrance conditions. Results from these studies will be described in forthcoming reports.

References

1. Zelazny, S.W., Driscoll, R.J., Raymonda, J.W., Blauer, J.A., Solomon, W.C., "Modeling DF/HF CW Lasers: An Examination of Key Assumptions," Vol. 16, No. 4, April 1978, pp. 297-304 (also AIAA preprint 77-63, January 1977).
2. Zelazny, S.W., Andrysiak, S.J., Furner, T.E., Rushmore, W.L., and Solomon, W.C., "Army Nozzle Technology Program, Vol II Chemical Pump Application (U)," Bell Aerospace Textron Report 9271-927003, MIRADCOM Report H-CR-78-7, March 1978 (Confidential).
3. Waypa, J., Hook, D.L., Reiner, R.J., and Zuryk, J.A., "Army Nozzle Technology Program," TRW Contract Report H-CR-77-14, October 1977 (Confidential).
4. Forbes, S.G., Trost, J.E., Ackerman, R.A., Clendening, C.W., "Long Range Chemical Laser Program," AFWL Report TR-77-144, TRW Contractor Report for Contract F29601-76-C-0014, March 1978.
5. Meinzer, R.A. et al, "Army Nozzle Technology Program," UTRC Report No. H-CR-78-2, November 1977 (Confidential).
6. "Long-Range Cold-Reaction HF Chemical Laser Program. Task 2 - Technology Investigations," AFWL Report in preparation by United Technologies Research Center, March 1978.
7. O'Keefe, , Sigimura, T., Behrens, W., Bullock, D., and Dee, D., "Comparison of LAMP and BLAZER Code Calculations with CL XV Measurements," Advances in Laser Technology (Emphasizing Gaseous Lasers), SPIE Vol. 138, 1978, pp. 116-125, 1978.
8. Driscoll, R.J., "Study of Boundary Layers in Chemical Laser Nozzles," AIAA Journal, Vol. 14, No. 11, November 1976, pp. 1571-1577.
9. Lankford, D.W. and Rapagnani, N.L., "Time Dependent Nozzle and Base Flow/Cavity Model of CW Chemical Laser Flowfields," AIAA Conference on Fluid Dynamics of High Power Lasers, Paper IV-3, 31 October - 2 November 1978.
10. Sentman, L.H., "Rotational Nonequilibrium in CW Chemical Lasers," Journal of Chemical Physics, Vol 62, 1975, pp. 3523.
11. Private Communication with N.L. Rapagnani at AFWL, Kirtland AFB, Albuquerque, NM.
12. Sentman, L.H., "Chemical Laser Power Spectral Performance: A Coupled Fluid Dynamic, Kinetic, and Physical Optics Model," Applied Optics, Vol 17, No. 14, July 1978, pp.2244-2249.

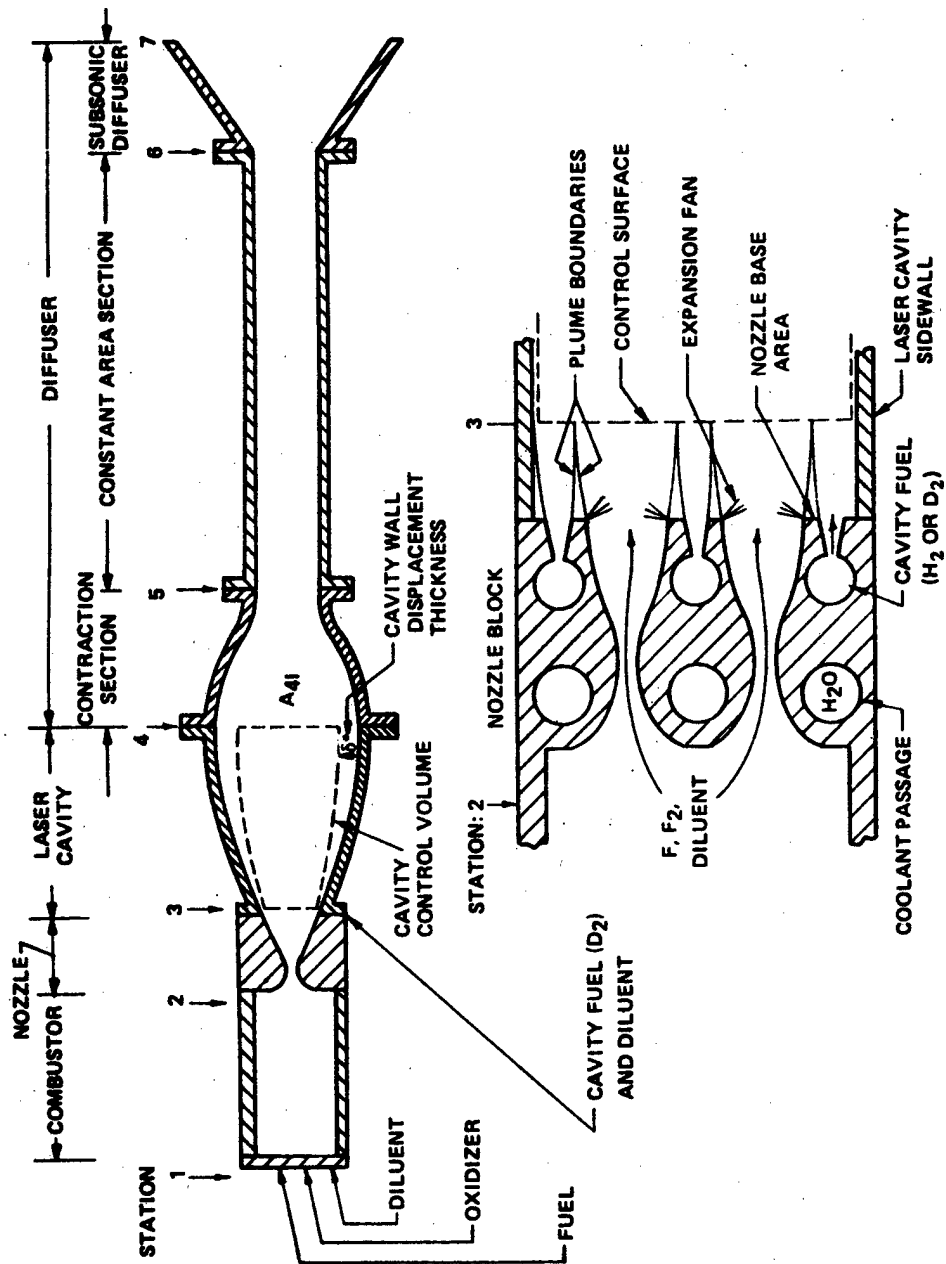


Figure 1. Flow System and Nozzle Geometry

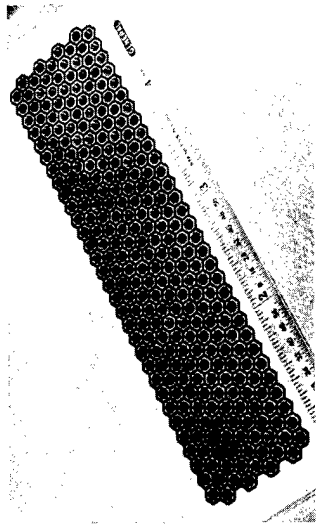


Figure 2a. BCL-7, 1 x 4 in., Low Base, High Pressure Chemical Laser Nozzle

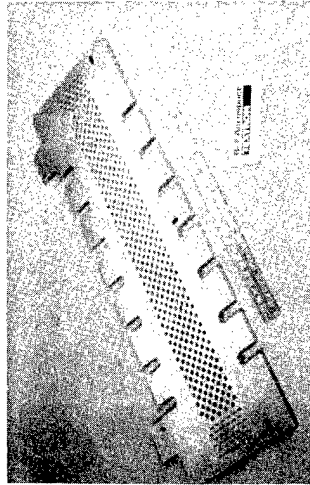


Figure 2b. BCL-13, 1 x 7 in., High Base, Low Pressure Chemical Laser Nozzle

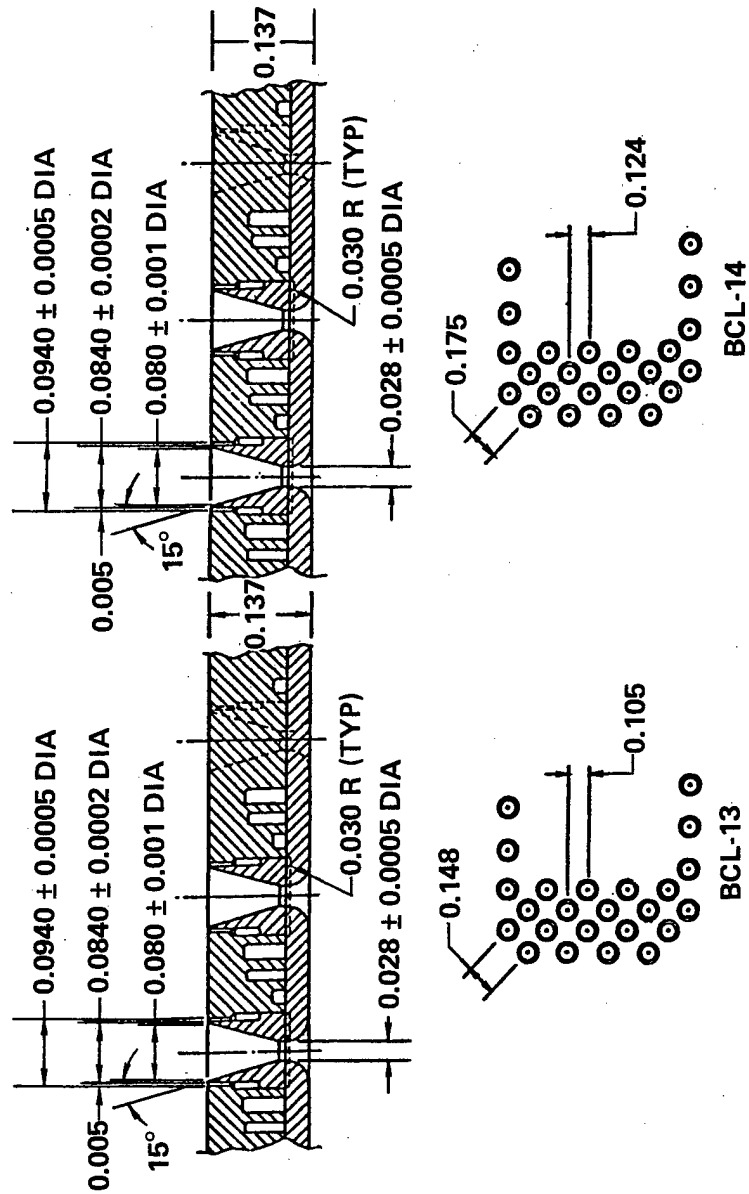


Figure 3. Schematics of Two High Base Axisymmetric Nozzles, BCL-13 and BCL-14

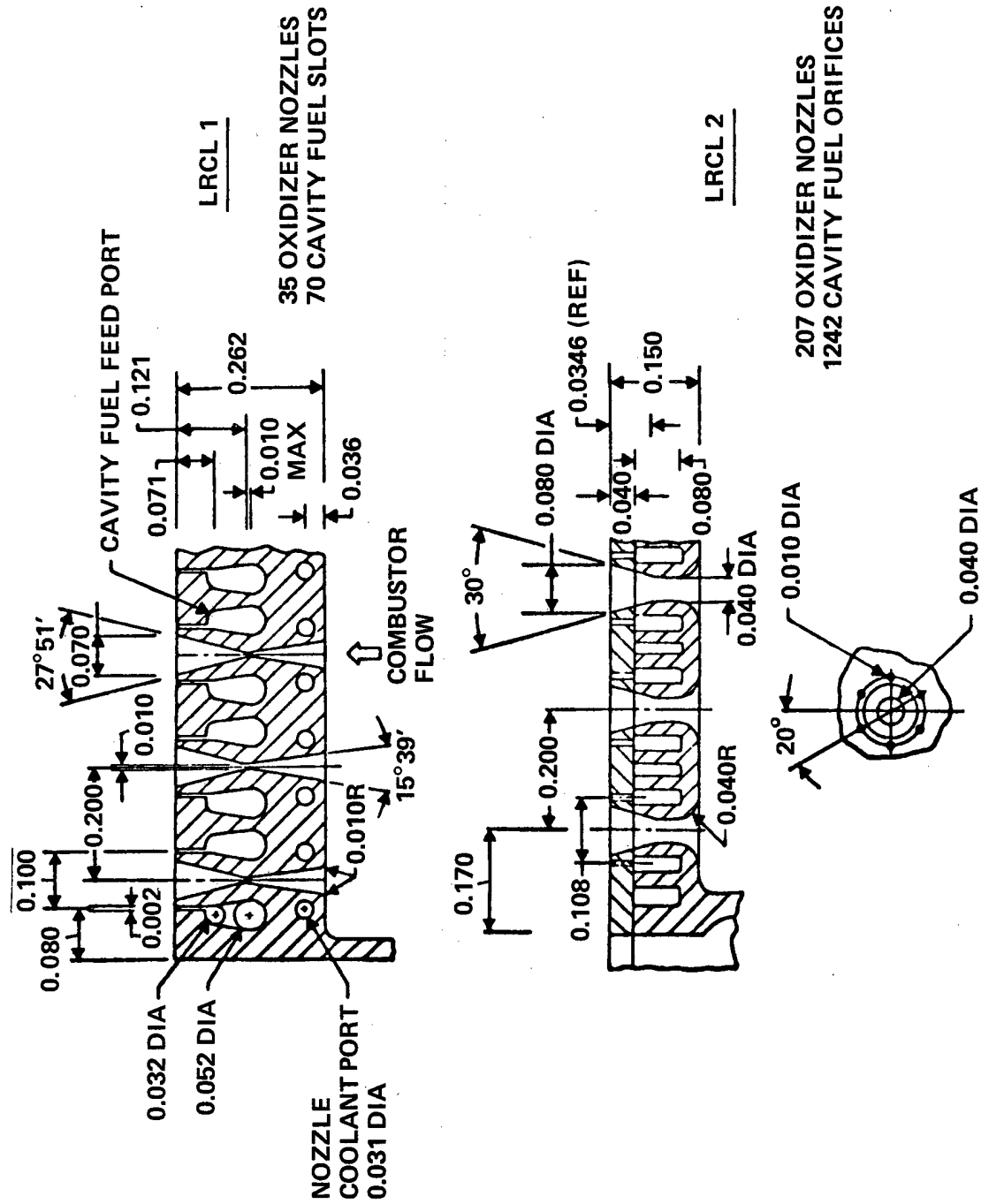


Figure 4. LRCL Advanced Nozzle Configurations

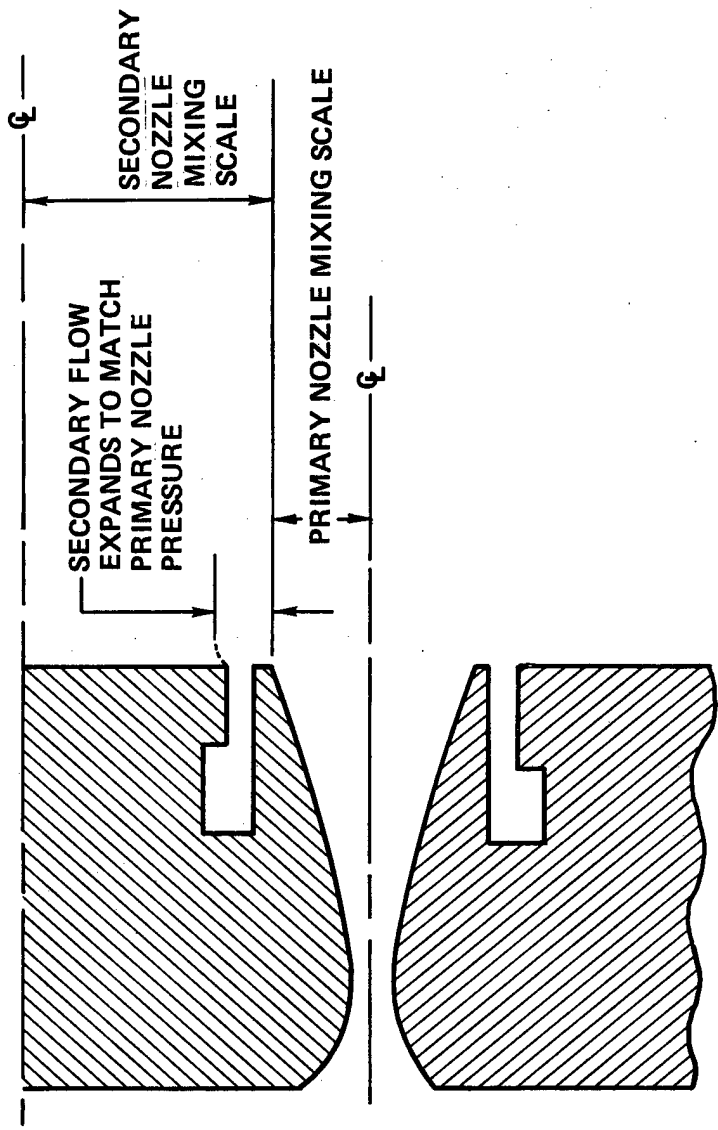


Figure 5. Sideview of 2D or Axisymmetric High Base Nozzle

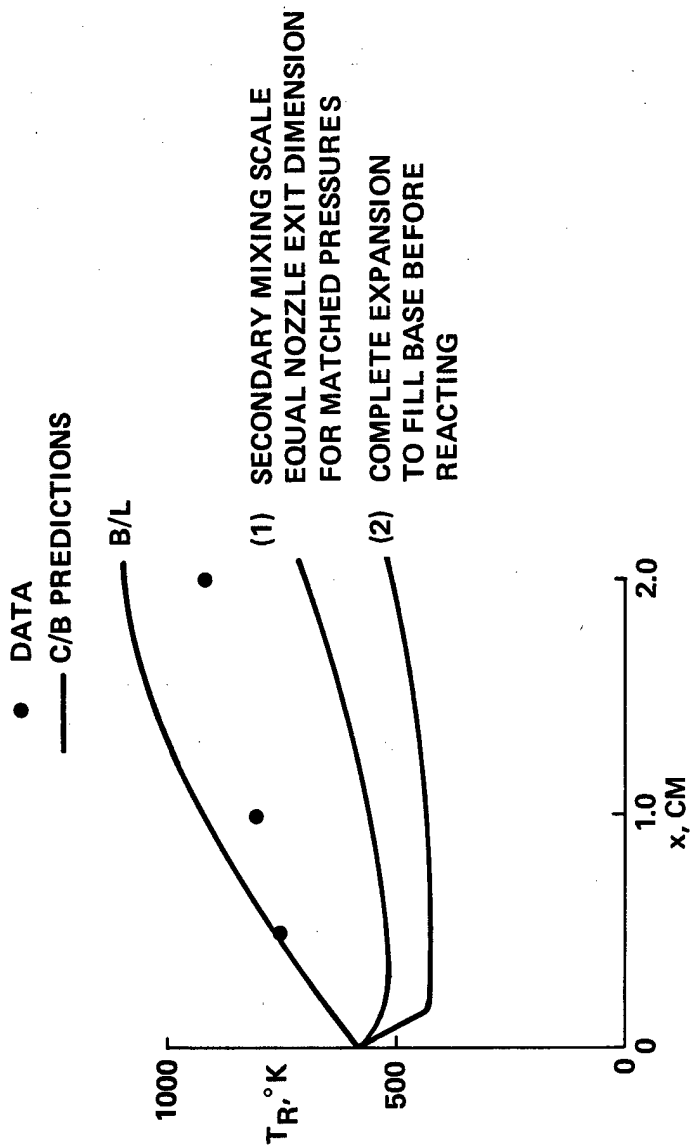


Figure 6. BCL-13 Chemiluminescence Data $T_{0I} = 4000^\circ K$, $\beta_{N_2} = 0.8$, $R_L = 14$, $\beta_s = 0$, $p'_7 = 27$ torr

BCL-13, BCL-14 - DF*

$T_{01} = 4000^\circ\text{K}$, $\beta_{N_2} = 0.8$, $R_L = 13$, $\beta_s = 0.0$

— **CNCDE PREDICTIONS WITH
80% NORMAL SHOCK RECOVERY**

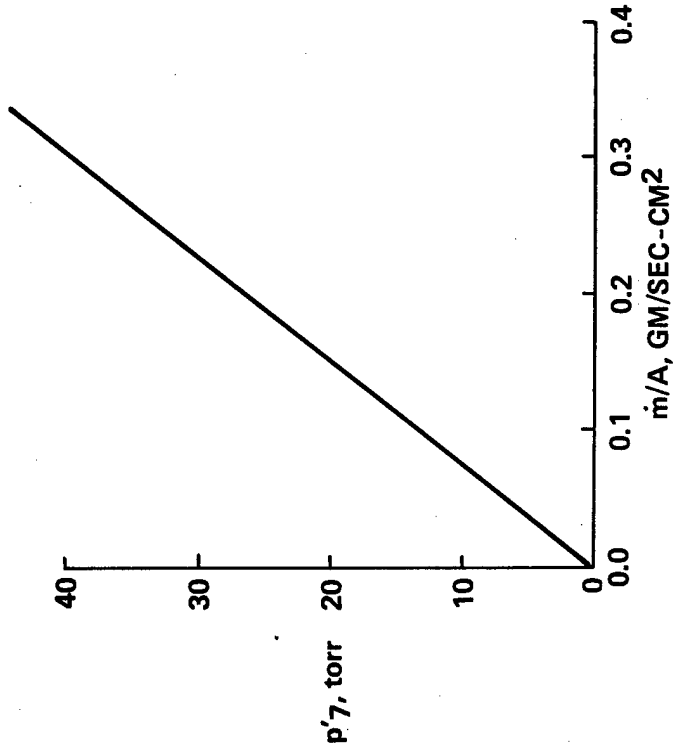


Figure 7. Variation of p'_7 with \dot{m}/A

$\dot{m}/A = 0.304 \text{ GM/SEC-CM}^2,$
 $T_{oc} = 2950^\circ\text{K}, \beta_{N_2} = 0.8, R_L = 13$

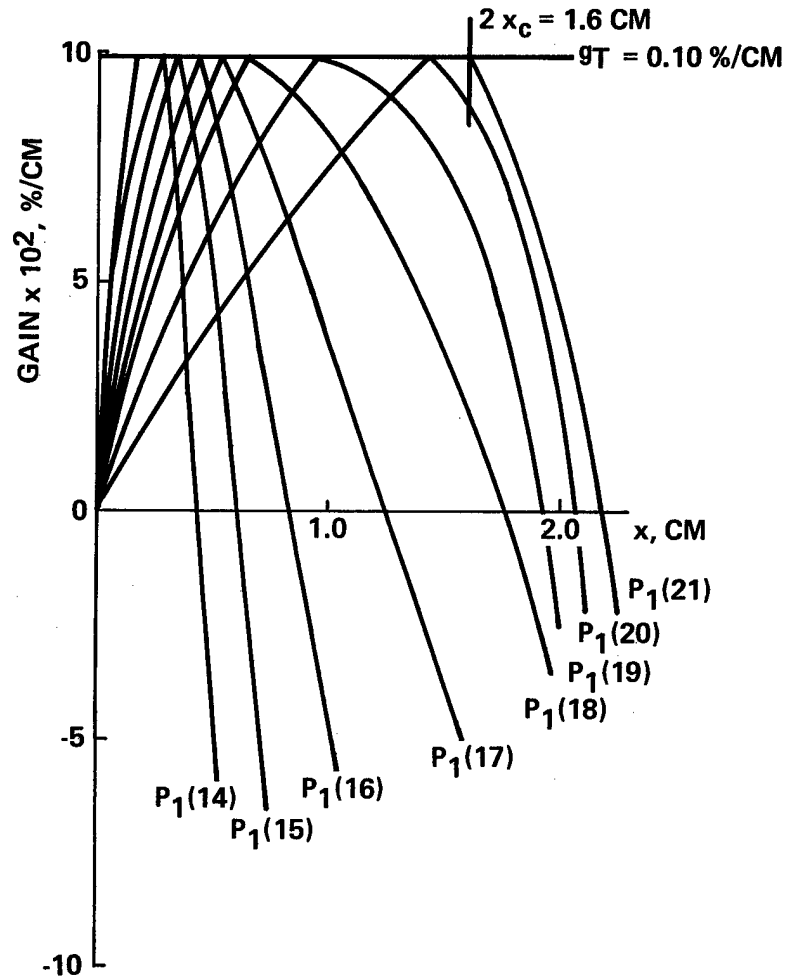


Figure 8. BCL-14 - DF* - P₁(J) Lines, Power On

$T_{O_1} = 4000^\circ\text{K}$, $\beta_{N_2} = 0.8$, $R_L = 13$, $\beta_s = 0$

\odot $\sim \bar{\sigma}^*$ DATA — C/B, COMPLETE RECOMBINATION
 \square $\sim x_c$ DATA - - - C/B, NO RECOMBINATION

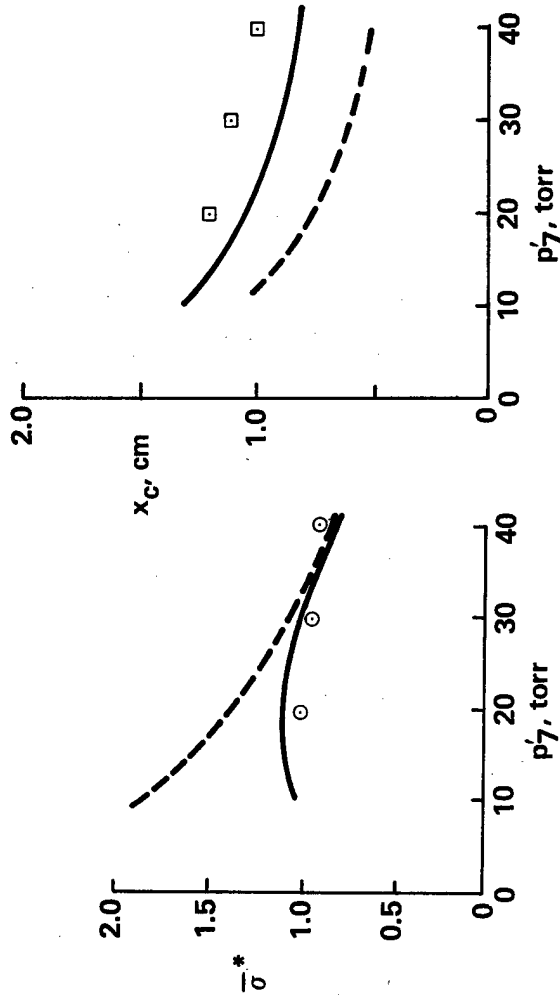


Figure 9, BCL-14 - DF* - p'_7 Scan

— C/B PREDICTION

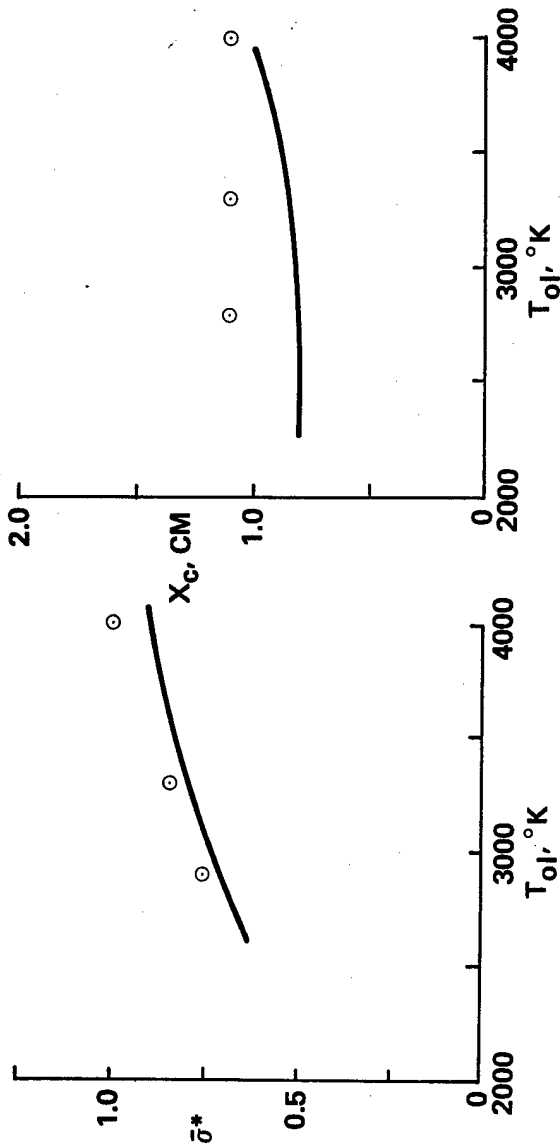


Figure 10. $\odot \sim$ BCL-14 Data, T_{0I} Scan at $p' = 27$ torr, $\beta_{N_2} = 1.0$, $R_L = 15$, $\beta_S = 0$

— C/B PREDICTIONS

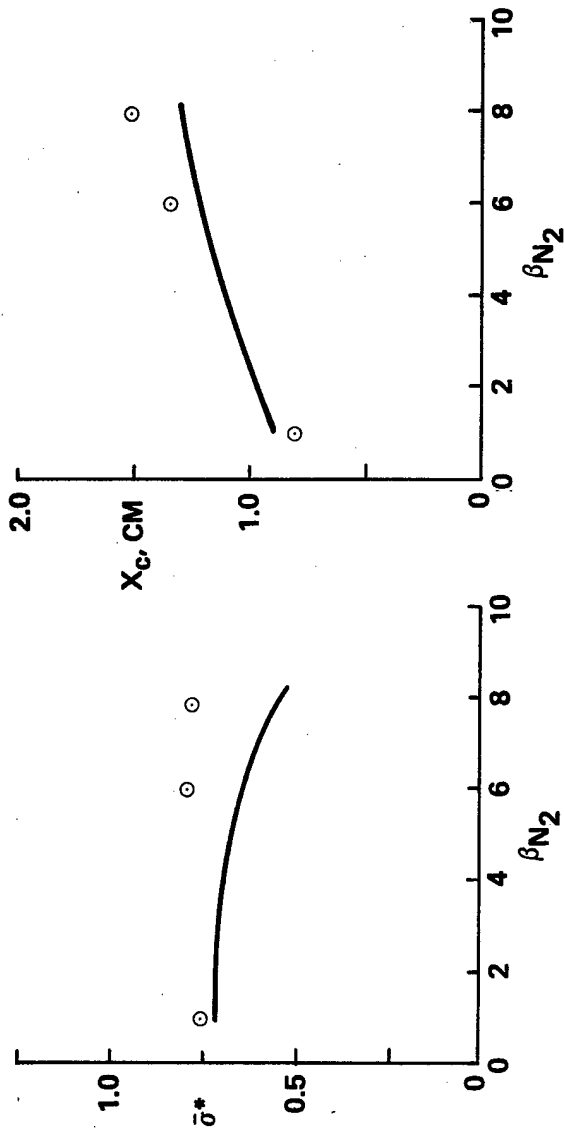


Figure 11. $\circ \sim$ BCL-14 Data. β_{N_2} Scan at $p'7 = 24$ torr, $T_{OI} = 2700^\circ K$, $R_L = 15$, $\beta_s = 0$

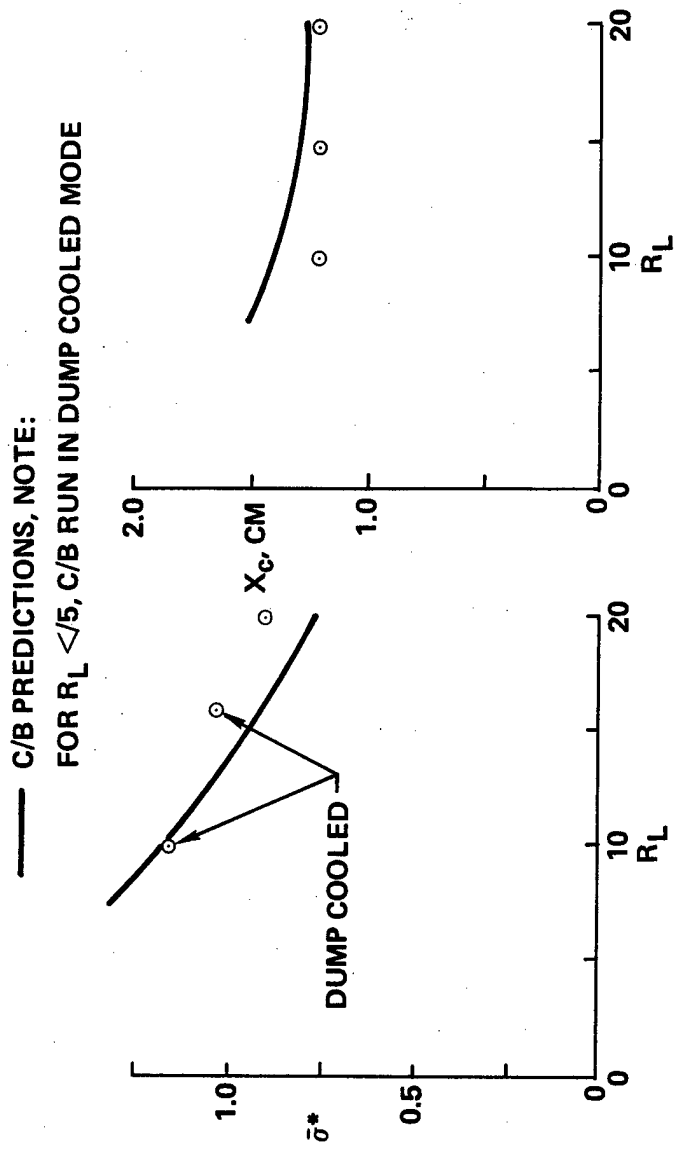


Figure 12. $\circ \sim$ BCL-14 Data, R_L Scan at $p_1' = 25$ torr, $T_{OI} = 4000^\circ\text{K}$, $\beta_{N_2} = 1.0$, $\beta_s = 0.0$

— C/B PREDICTIONS

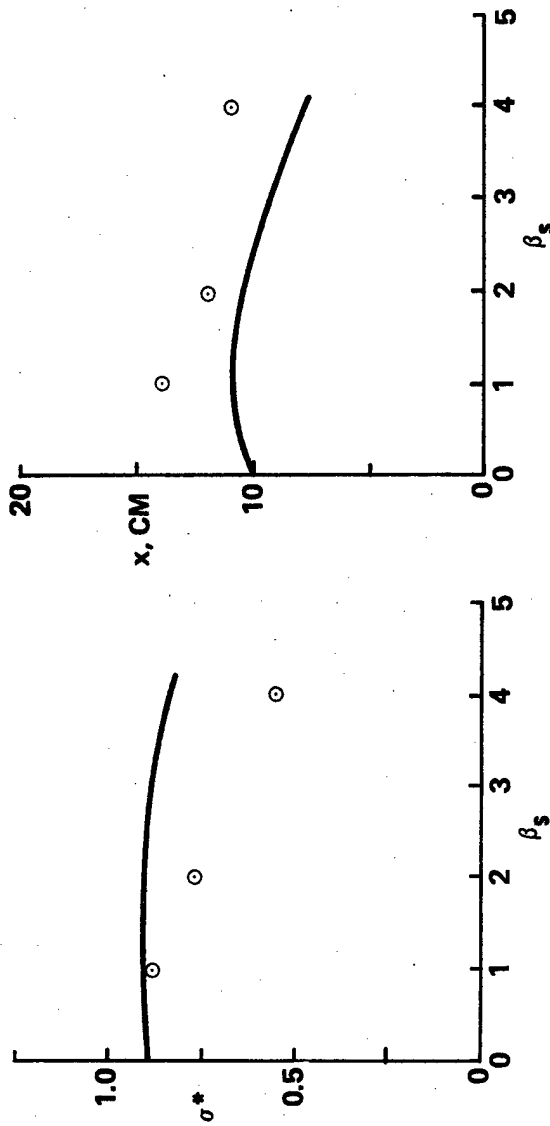


Figure 13. $\circ \sim$ BCL-14 Data, β_s Scan at $p' = 27$ torr, $T_{oI} = 4000^\circ\text{K}$, $\beta_{N_2} = 1.0$, $R_L = 15$

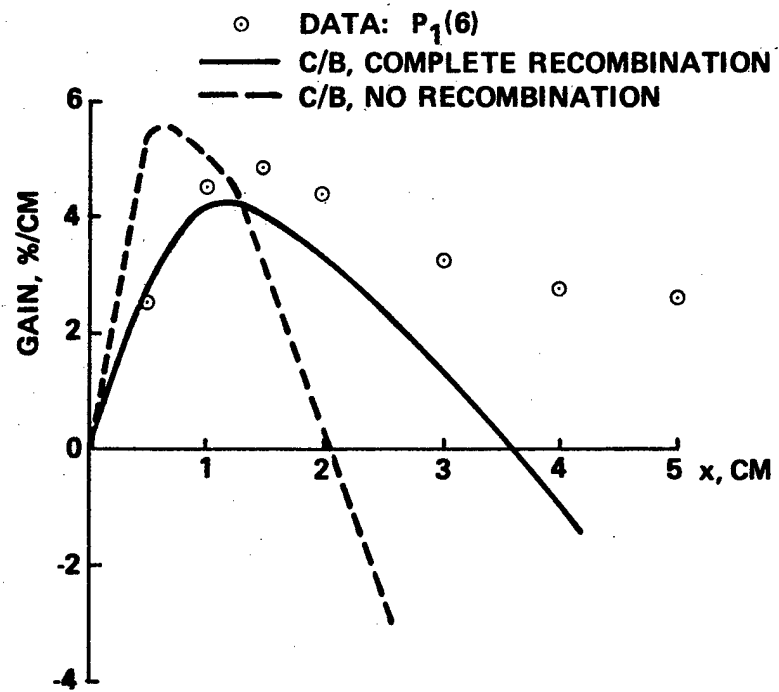


Figure 14. LRCL-2, Condition 501, $\dot{m}/A = 0.042 \text{ gm/sec-cm}^2$

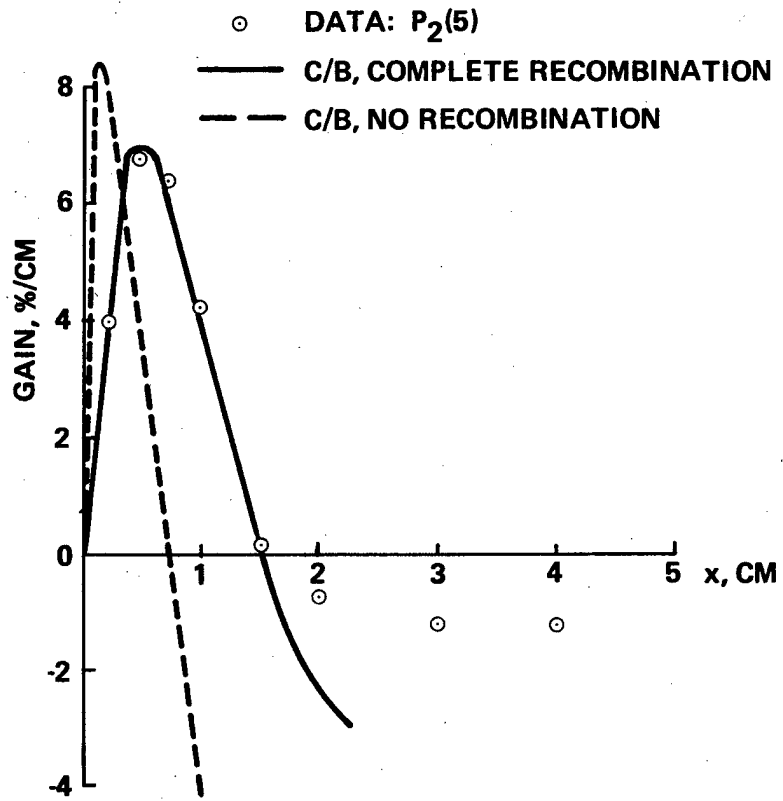


Figure 15. LRCL-2, Condition 501, $\dot{m}/A = 0.042 \text{ gm/sec-cm}^2$

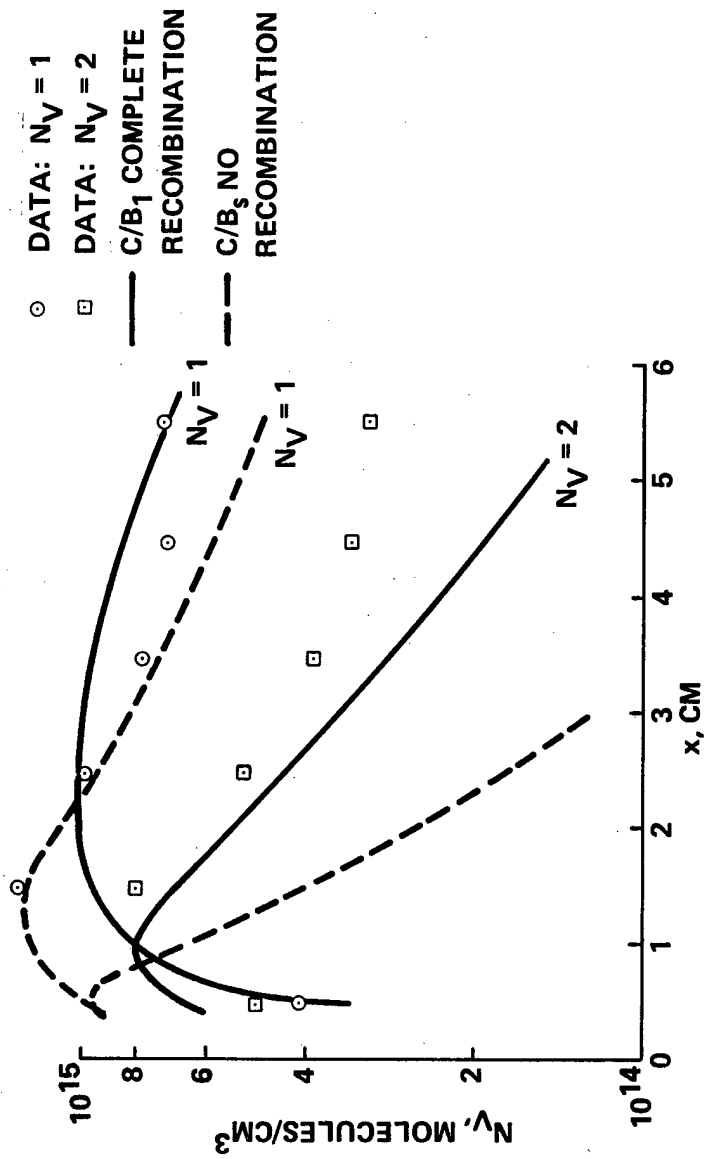


Figure 16. LRCL-2, Condition 500, $\dot{m}/A = 0.042$ gm/sec-cm²

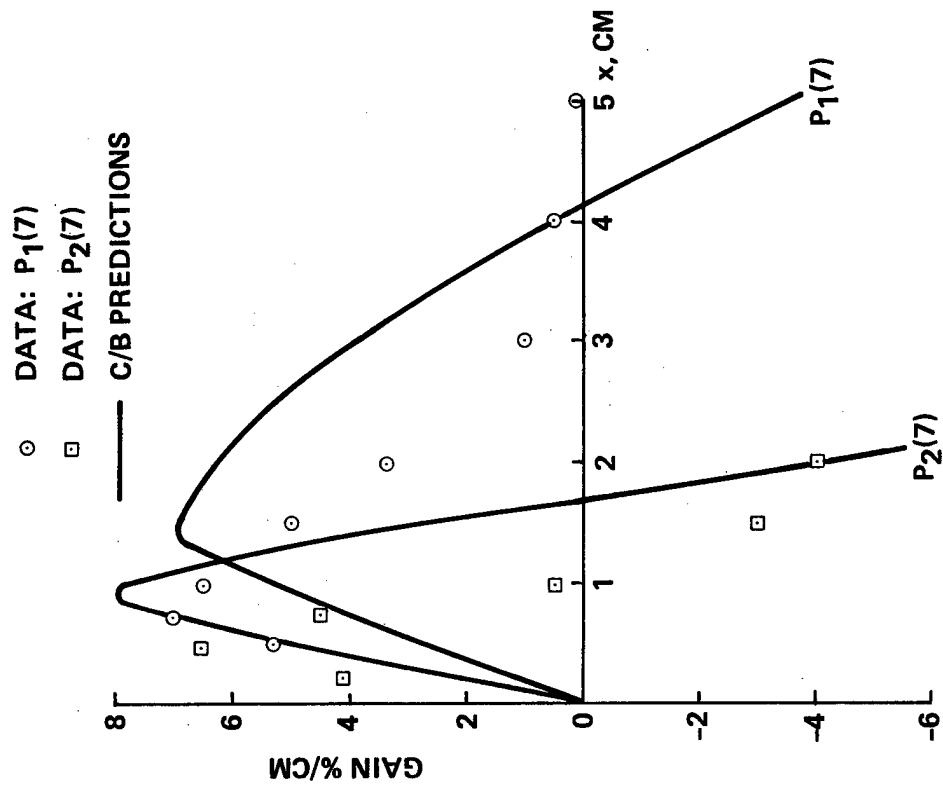


Figure 17. LRCL-1, \dot{m} 1A = 0.147 gm/sec - cm²

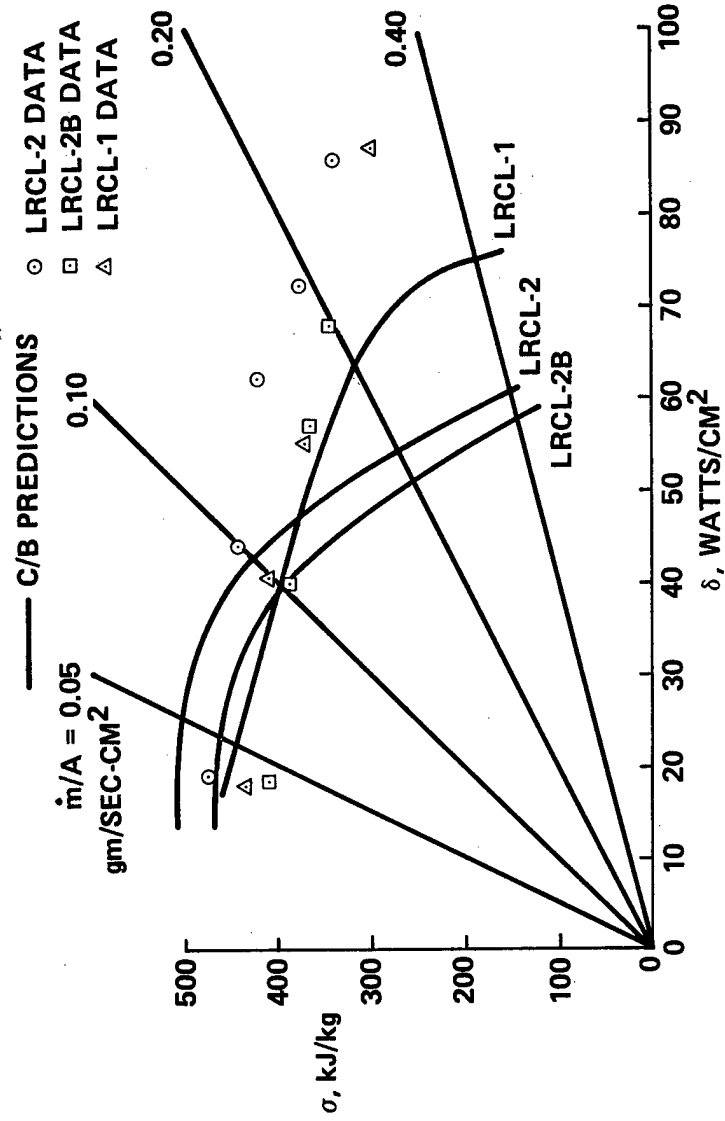


Figure 18. LRCL Free Jet Performance

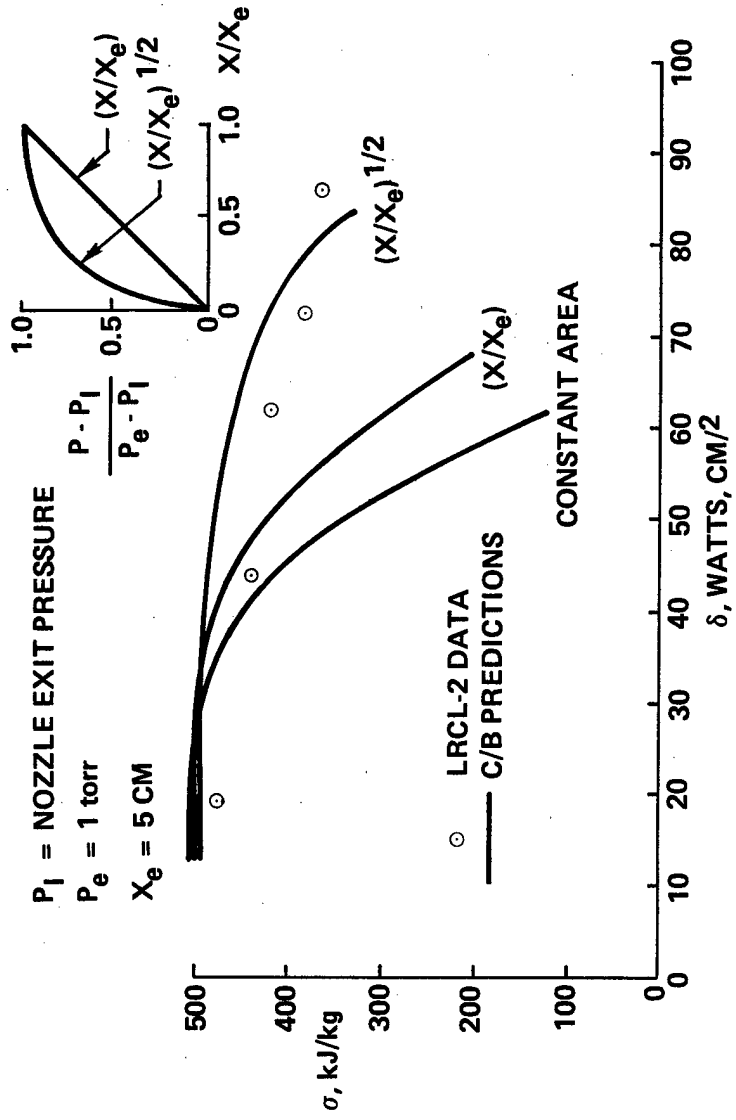


Figure 19. Effect of Cavity Boundary Condition

TABLE 1. MODELING CW DF AND DF LASERS DATA BASE

NOZZLE ID	NOZZLE TYPE	TYPE OF DATA	DILUENT- LASING MOLECULE
BCL-13	AXI	CCP, CHEMILUM.	N ₂ - DF*
BCL-14	AXI	CCP	N ₂ - DF*
LRCL-1	2D	CCP, ZPG	He - HF*
LRCL-2	AXI	CCP, ZPG	He - HF*
LRCL-2B	AXI	CCP	He - HF*

TABLE 2a. REACTION RATE(1) DATA FOR D₂-F₂ SYSTEMS (1978); REACTIONS INVOLVING GENERALIZED COLLISION PARTNERS

Reaction	M(2)	A	N	E (kcal)	Comments
F ₂ = F + F	*2.4F ₂ , 2.4F	5 x 10 ¹³	0.0	35.1	V = 0, 1, 2, 3
D + D = D ₂ (V)	*0D ₂ , 0D	1 x 10 ¹⁸	-1.0	0.0	V = 0, 1, 2, 3
D + D = D ₂ (V)	D	3 x 10 ¹⁷	-0.5	0.0	V = 0, 1, 2, 3
D + D = D ₂ (V)	D ₂	1 x 10 ¹⁷	-0.67	0.0	V = 0, 1, 2, 3
D ₂ (V) = D ₂ (V-1)	*5D ₂ , 0D	1.8V x 10 ⁻³	4.3	0.0	V = 1, 2, 3
D ₂ (V) = D ₂ (V')	D	1.6 x 10 ¹⁵	-0.9	2.4	V = 1, 2, 3
DF(V) = D + F	*5D, 5F, 5DF, 0D ₂ , 5HF	1.2 x 10 ¹⁸	-1.0	0 ^a -E _{vib}	0 ≤ V' < V
DF(V) = DF (V')	DF, 1.58 HF	1.2V x 10 ¹⁴	-1.0	0.0	0 ≤ V ≤ 9
DF(V) = DF (V-1)	DF, HF	1.4V x 10 ²	+2.96	0.0	1 ≤ V ≤ 9, 0 ≤ V' < V, Low Temperature Form
DF(V) = DF (V-1)	D ₂ , 5CF ₄	5.5V x 10 ¹	+3.0	0.0	1 ≤ V ≤ 9, High Temperature Form
DF(V) = DF (V-1)	F ₂ , 2He, N ₂ , Ar	7.8V x 10 ⁻⁷	+5.0	0.0	1 ≤ V ≤ 9
DF(V) = DF (V-1)	F	1.6V x 10 ¹³	0.0	3.38	1 ≤ V ≤ 9
DF(1) = DF (0)	D	2.4 x 10 ¹¹	0.0	1.22	1 ≤ V ≤ 9
DF(V) = DF (V-1)	D	6.9 x 10 ¹¹	0.0	1.38	V = 2, 3
DF(V) = DF (V-1)	D	8.6 x 10 ¹³	0.0	1.38	4 ≤ V ≤ 9
DF(V) = DF (V')	D	6.9 x 10 ¹¹	0.0	1.38	3 ≤ V ≤ 9, 0 ≤ V' ≤ V-2
N ₂ (1) = N ₂ (0)	DF, HF	2.3 x 10 ¹	+3.3	-0.70	
N ₂ (1) = N ₂ (0)	*0DF, 0HF	1.2 x 10 ⁸	0.0	12.3	

(1) The reaction rate constants are expressed in the form $k = AT^N \exp(-E/RT)$. Units are $\text{cm}^3 \cdot \text{mol}^{-1} \cdot \text{sec}^{-1}$.

(2) The symbol * means all species act as third bodies with unit efficiency.

The symbol $r/R, s/S$ means that all species act as third bodies with unit efficiency except R and S, which act with efficiencies r and s respectively.

The symbol rR, sS, \dots means that the rate so labeled is only for species R, S, ... acting as third bodies with efficiencies r, s, \dots respectively.

TABLE 2b. EXCHANGE AND PUMPING REACTION RATE (1) DATA FOR
D₂-F₂ SYSTEMS (1978)

Reaction	A	N	E(kcal)	Comments
F + D ₂ = DF(V) + D	k x 10 ¹³	0.0	1.97	k = 1.76, 4.0, 6.0, 4.32 for V = 1, 2, 3, 4
D + DF(V) = D ₂ (V) + F	1.0 x 10 ¹³	0.0	0.5	5 ≤ V ≤ 9, 0 ≤ V' ≤ 3
D + F ₂ = DF(V) + F	k x 10 ¹³	0.0	2.46	k = 0.48, 1.02, 1.70, 2.72, 0.82, for V = 5, 6, 7, 8, 9
DF(V) + DF(V') = DF(V-1) + DF(V'+1)	6 x 10 ¹⁵	-1.0	0.0	1 ≤ V, V' ≤ 8
D ₂ (V) + DF(V') = D ₂ (V-1) + DF(V'+1)	k x 10 ¹³	0.0	0.0	V = 1, 2, 3; k = 0.173, 0.54, 1.2, 2.5, 4.9, 9.7, 19.4, 39.0 for V' = 1, 2, 3, 4, 5, 6, 7, 8
D ₂ (1) + D ₂ (V) = D ₂ (0) + D ₂ (V+1)	k x 10 ⁷	1.5	0.0	k = 1.14, 1.64, for V = 1, 2

(1) The reaction rate constants are expressed in the form $k = AT^N \exp(-E/RT)$. Units are cm³·mol⁻¹·sec⁻¹.

TABLE 3a. REACTION RATE⁽¹⁾ DATA FOR THE H₂-F₂ CHEMICAL SYSTEM (1978);
REACTIONS INVOLVING GENERALIZED COLLISION PARTNERS

Reactions	M (2)	A	N	E (kcal)	Comments
H+H = H ₂ (V)	*/H, H ₂	6.2 x 10 ¹⁷	-0.95	0.0	V ≤ 3
H+H = H ₂ (V)	H ₂ , 2.0 H	9.4 x 10 ¹⁶	-0.61	0.0	V ≤ 3
F+F = F ₂	*/2.4 F ₂ , 2.4 F	4.71 x 10 ¹⁵	-1.0	-1.25	
H ₂ (V) = H ₂ (V-1)	*/H ₂ , H	2.5 x 10 ⁴ V	4.3	0.0	V ≤ 3
H ₂ (V) = H ₂ (V-1)	H ₂ , H	1.0 x 10 ⁻³ V	4.3	0.0	V ≤ 3
H ₂ (V) = H ₂ (V-1)	H	2.0 x 10 ¹³	0.0	2.72	V ≤ 3
HF(V) = HF(V-1)	HF+0.5 DF	2.95 x 10 ¹⁴ V	-1.0	0.0	V ≤ 7
HF(V) = HF(V-1)	HF+0.5 DF	3.5 x 10 ⁴ V	2.26	0.0	V ≤ 7
HF(V) = HF(V-2)	HF+0.5 DF	7.5 x 10 ¹⁴ (V-1)	-1.0	0.0	V ≤ 7
HF(V) = HF(V-3)	HF+0.5 DF	5.0 x 10 ¹⁴ (V-1)	-1.0	0.0	V ≤ 7
HF(V) = HF(V')	H	4.5 x 10 ¹² g(V)	0.0	0.7	V' < , g(1) = 0.1 g(V > 1) = 1.0
HF(V) = HF(V-1)	Ar, F ₂ , 2(He, N ₂ , CF ₄)	7.7 x 10 ⁻⁷ V	5.0	0.0	V ≤ 7
HF(V) = HF(V-1)	H ₂	6.0 x 10 ⁷ V	1.0	0.0	V ≤ 7
HF(V) = HF(V-1)	F	1.93 x 10 ¹⁶ g(V)	-0.75	3.6	g(V) = V ^{1.37}
HF(V) = HF(V-2)	F	9.64 x 10 ¹⁵ g(V)	-0.75	3.6	g(V) = V-1 ^{1.34}
HF(V) = HF(V-3)	F	1.45 x 10 ¹⁶ g(V)	-0.75	3.6	g(V) = V-2 ^{0.9}

(1) See Table 2a Footnote 1

(2) See Table 2a Footnote 2

TABLE 3b. EXCHANGE PUMPING AND REACTION RATE⁽¹⁾ DATA
FOR H₂-F₂ SYSTEMS (1978)

Reactions	A	N	E (Kcal)	Comments
F + H ₂ (V') = HF (1) + H	2.72 x 10 ¹³	0.0	1.6	V' ≤ 3
F + H ₂ (V') = HF (2) + H	8.79 x 10 ¹³	0.0	1.6	V' ≤ 3
F + H ₂ (V') = HF (3) + H	4.48 x 10 ¹³	0.0	1.6	V' ≤ 3
H + HF(4) = H ₂ (V) + F	3.70 x 10 ¹²	0.0	0.46	V ≤ 1
H + HF (5) = H ₂ (V) + F	3.87 x 10 ¹² g (V)	0.0	0.51	g(0) = 1, g(2) = 1.78
H + HF (6) = H ₂ (V) + F	4.17 x 10 ¹²	0.0	0.58	V ≤ 3
H + F ₂ = HF (3)	1.2 x 10 ¹⁴ g(V)	0.0	2.4	g (V) = .08, .13, .35, .44, for V = 3, 4, 5, 6
HF (V) + HF (V') = HF (V-1) + HF (V' + 1)	3.0 x 10 ⁵	-1.0	0.0	ΔV = V - V' ≤ 3
H ₂ (V) + HF(0) = H ₂ (V-1) + HF(1)	8.3 x 10 ¹¹ g(V)	0.0	0.0	g(V) = 1, 3.3, 10, 23, 46, 90, for V = 0, 1, 2, 3, 4, 5
H ₂ (V) + H ₂ (V') = H ₂ (V-1) + H ₂ (V'+1)	3.5 x 10 ⁶ V(V'+1)	1.5	0.0	V, V' ≤ 3

1. See Table 2a Footnote 1.
2. See Table 2a Footnote 2.

**TABLE 4. COMPARISON BETWEEN THEORY AND DATA FOR THE BCL-13
REGENERATIVELY COOLED AXISYMMETRIC NOZZLE**

(a) Test Conditions

\dot{m}/A , gm/sec-cm ²	0.249
T_{oc} , °K	2721
β_c	0.80
β_s	0.50
R_L	13.0

(b) Theory and Data Comparison

	<u>Predicted</u>	<u>Measured</u>
Lasing Zone Length, cm	1.10	0.86
Relative Power	1.0	0.98

TABLE 5. COMPARISON OF MEASURED AND PREDICTED X_c FOR LRCL NOZZLES

Nozzle	\dot{m}/A gm/sec-cm ²	X_c cm		$(X_c) C/B$
		Data	C/B	$(X_c) Data$
LRCL-1	0.0412	1.77	1.15	0.65
	0.0988	2.50	1.20	0.48
	0.1472	2.45	1.24	0.51
	0.2865	2.98	1.50	0.50
	0.3468	2.95	1.85	0.63
LRCL-2B	0.0430	0.99	1.40	1.41
	0.1033	2.92	2.00	0.68
	0.1546	2.94	1.60	0.54
	0.1954	3.41	1.50	0.44
LRCL-2 ⁽¹⁾	0.0405	1.50	0.95	0.63
	0.1002	1.48	1.02	0.70
	0.1480	1.99	1.07	0.54
	0.1920	1.97	1.05	0.53
	0.2529	2.46	0.88	0.36
LRCL-2 ⁽²⁾	0.0405	1.50	1.20	0.80
	0.1002	1.48	1.24	0.84
	0.1480	1.99	1.70	0.85
	0.1920	1.97	2.30	1.17
	0.2529	2.46	1.60	0.65

(1) Constant Area Cavity Boundary Condition

(2) $\frac{P - P_i}{P_e - P_i} = \left(\frac{X}{X_e} \right)^{1/2}$ Cavity Boundary Condition

TABLE 6. HF MODELING SENSITIVITY TO REACTION RATE VARIATIONS.
TEST CASE IS FOR LRCL-2 NOZZLE, RUN NO. 1 + B6-2868

C/B Run	Rate Constant Examined and How Varied	At Cutoff			
		$2X_c$	σ	$2\bar{X}_c$	$\bar{\sigma}$
1	Baseline	1.80	512	1.00	1.00
2a	Pumping Reaction Rates x 2	1.60	515	0.89	1.01
2b	Pumping Reaction Rates x 1/2	1.80	497	1.00	0.97
3	HF/HF V-T *2	1.60	486	0.89	0.95
4	HF/DF V-T *2	1.60	494	0.89	0.96
5	HF/H V-T *2	1.80	479	1.00	0.94
6	HF/HF V-V *2	1.60	500	0.89	0.98
7	HF/H2 V-V *2	1.40	473	0.78	0.92

Nomenclature:

Barred quantities are non-dimensionalized by their baseline values.

Cutoff is point where first four levels reach maximum power.

($\dot{m}/A = 0.0405$ gm/sec-cm², $T_{oc} = 2126^\circ K$, $\psi_c = 3.96$, $R_L = 11.5$, $\beta_s = 0.0$)

EXPERIMENTAL $X_c = 1.50$ CM, $\sigma = 474$ kJ/kgm